



저작자표시-비영리-변경금지 2.0 대한민국

이용자는 아래의 조건을 따르는 경우에 한하여 자유롭게

- 이 저작물을 복제, 배포, 전송, 전시, 공연 및 방송할 수 있습니다.

다음과 같은 조건을 따라야 합니다:



저작자표시. 귀하는 원저작자를 표시하여야 합니다.



비영리. 귀하는 이 저작물을 영리 목적으로 이용할 수 없습니다.



변경금지. 귀하는 이 저작물을 개작, 변형 또는 가공할 수 없습니다.

- 귀하는, 이 저작물의 재이용이나 배포의 경우, 이 저작물에 적용된 이용허락조건을 명확하게 나타내어야 합니다.
- 저작권자로부터 별도의 허가를 받으면 이러한 조건들은 적용되지 않습니다.

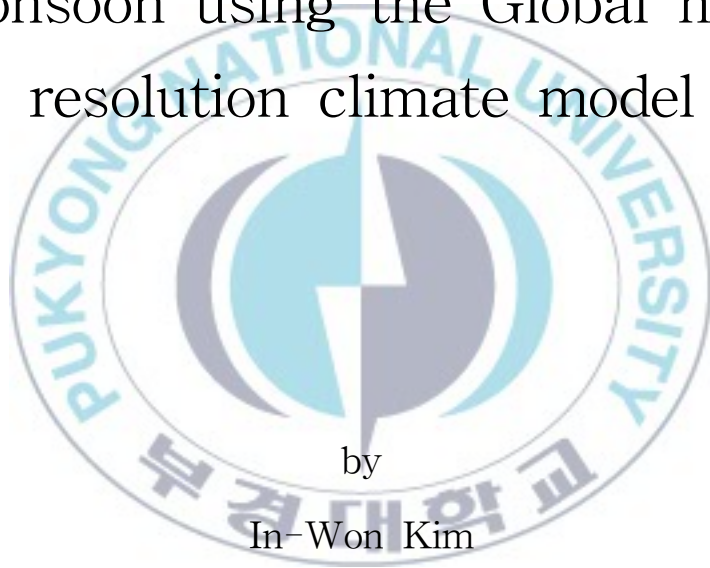
저작권법에 따른 이용자의 권리는 위의 내용에 의하여 영향을 받지 않습니다.

이것은 [이용허락규약\(Legal Code\)](#)을 이해하기 쉽게 요약한 것입니다.

[Disclaimer](#)

Thesis for the Degree of Master of Science

Study on impacts of IOD and
ENSO on East Asian summer
monsoon using the Global high
resolution climate model



by

In-Won Kim

Department of Environmental Atmospheric Science

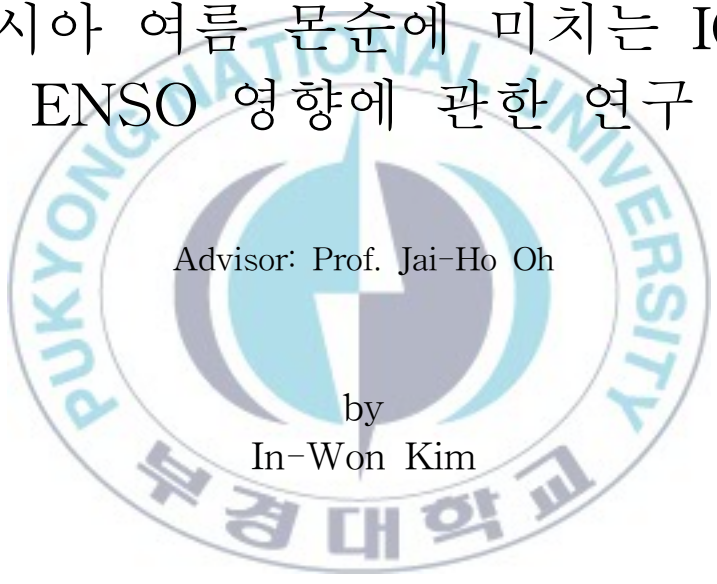
The Graduate School

Pukyong National University

February 2012

Study on impacts of IOD and ENSO on East Asian summer monsoon with using the Global high resolution climate model

전지구 상세기후모델을 이용한
동아시아 여름 몬순에 미치는 IOD와
ENSO 영향에 관한 연구



Advisor: Prof. Jai-Ho Oh

by

In-Won Kim

A thesis submitted in partial fulfillment of the requirements
for the degree of

Master of Science

in Department of Environmental Atmospheric Sciences, The
Graduate School,
Pukyong National University

February 2012



Study on impacts of IOD and ENSO
on East Asian summer monsoon
using the Global high resolution climate model

A dissertation
by
In-Won Kim

Approved by:



(Chairman)

Hyeong-Bin Cheong



(Member)

Umesh Singh



(Member)

Jai-Ho Oh

February 24, 2012

Contents

List of Figures	II
List of Tables	V
Abstract	VI
1. Introduction	1
2. Present-day Climate simulation Analysis	3
2. 1. Model description	3
2. 2. Data and methodology	7
2. 3. Rainfall variability over East Asia	9
2. 4. Relationship of IOD and ENSO upon snow depth	14
2. 5. Relationship between snow depth and rainfall	18
2. 6. Circulation associated with heavy snow	23
2. 7. Relationship of IOD and ENSO on surface temperature	27
3. Sensitivity experiments	29
3. 1. Experiment design	29
3. 2. Result of experiments	36
3. 2. 1. Rainfall distribution over East Asia	36
3. 2. 2. Snow depth distribution over East Asia	38
3. 2. 3. Circulation associated with IOD and ENSO	40
4. Summary and Conclusions	43
5. References	45

List of Figures

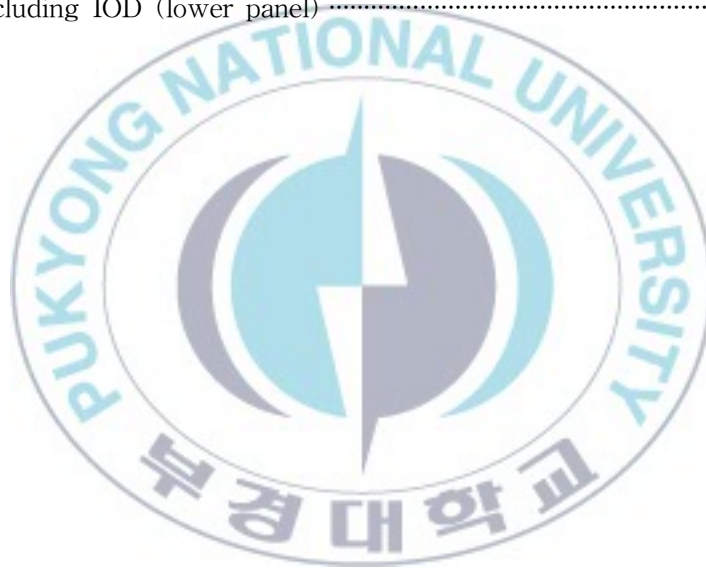
Fig. 2.1. Grid generation by successively halving the triangle edges to form new triangles. Parameter n_i is the number of intervals on major triangle edge	5
Fig. 2.2. Classification of years when positive or negative IOD and El Niño or La Niña occurred	8
Fig. 2.3. Composite precipitation anomalies in millimeters for the positive minus negative dipole events; (a) the concurrent year summer (b) following year summer	10
Fig. 2.4. Same as Fig. 2.3. but for the El Niño minus La Niña events; (a) the concurrent year summer (b) following year summer	10
Fig. 2.5. Correlation coefficients between the seasonal IODM and ENSO indices with area-mean summer precipitation; (a) Korea (b) Japan IODM-ENSO (ENSO-IODM) illustrates the partial correlation coefficient with IODM (ENSO) after removing the effect of ENSO (IODM)	13
Fig. 2.6. Composite snow depth anomalies in centimeters for the positive minus negative dipole events; (a) DJF0, (b) MAM+1	15
Fig. 2.7. Area-mean winter and spring snow depth; (a) over 50°N-60°N, 130°E-140°E region during the DJF0, (b) over 50°N-60°N, 130°E-140°E region during the MAM+1, (c) over 50°N-60°N, 50°E-100°E region during the DJF0, (d) over 50°N-60°N, 50°E-100°E region during the MAM+1	17
Fig. 2.8. Standardize snow depth over the area D and Rainfall over area B	

from 1979 to 2008	24
Fig. 2.9. Composite seasonal differences of 500hPa geopotential height in meters for the extreme now depth events (heavy minus light snow over area D)	26
Fig. 2.10. Correlation coefficients between the seasonal IODM and ENSO indices with area-mean summer surface temperature; (a) Korea (b) Japan IODM-ENSO (ENSO-IODM) illustrates the partial correlation coefficient with IODM (ENSO) after removing the effect of ENSO (IODM)	28
Fig. 3.1. Map showing the region of analysis	31
Fig. 3.2. IOD Index (upper panel) and Niño3 Index (lower panel) from 1960 to 1999	31
Fig. 3.3. Composite SST anomalies associated with IOD and ENSO; (a) Positive Dipole and El Niño case (b) El Niño only case (c) Negative Dipole and El Niño case (d) Positive Dipole only case (e) Climatology from 1960 to 1999 (f) Negative Dipole only case (g) Positive Dipole and La Niña case (h) La Niña only case (i) Negative Dipole and La Niña case	33
Fig. 3.4. Schematic representation of design of (a) Control run and (b) sensitivity experiments.	35
Fig. 3.5. Fig. 3.5 Rainfall difference in millimeters during the following summer (JJA+1) by present climate simulation (left panel) and sensitivity experiments (right panel); (a) Positive dipole minus Negative IOD phase excluding ENSO (b) El Niño minus La Niña phase excluding IOD	37
Fig. 3.6. Snow depth difference in centimeter during the winter and spring by sensitivity experiments; Positive dipole minus Negative IOD phase	

excluding El Niño (upper panel) and El Niño minus La Niña phase
excluding IOD (lower panel) 39

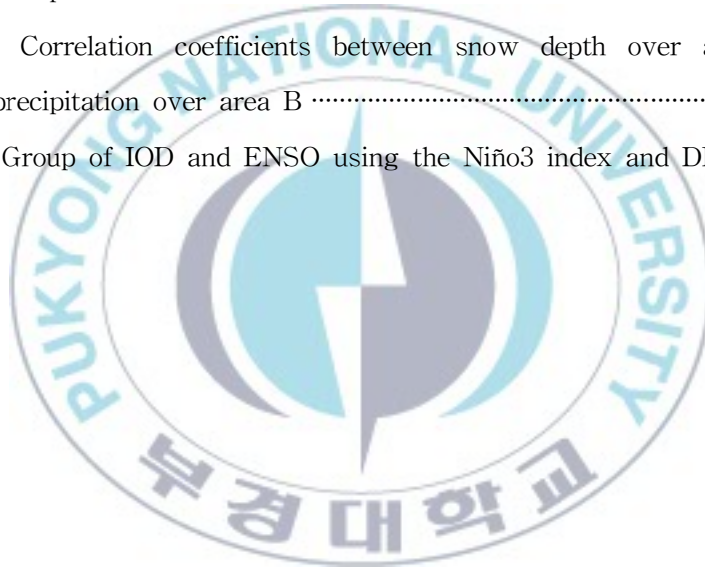
Fig. 3.7. 500 hPa geopotential height difference in meter during the Summer
by sensitivity experiments; Positive dipole minus Negative IOD phase
excluding El Niño (upper panel) and El Niño minus La Niña phase
excluding IOD (lower panel) 41

Fig. 3.8. 850 hPa Wind vector difference in m/s during the Summer by
sensitivity experiments; Positive dipole minus Negative IOD phase
excluding El Niño (upper panel) and El Niño minus La Niña phase
excluding IOD (lower panel) 42



List of Tables

Table 2.1. Summary of physical parameterization methods in GME	6
Table 2.2. Correlation coefficients between snow depth over area C and precipitation over area A	19
Table 2.3. Correlation coefficients between snow depth over area C and precipitation over area B	20
Table 2.4. Correlation coefficients between snow depth over area D and precipitation over area A	21
Table 2.5. Correlation coefficients between snow depth over area D and precipitation over area B	22
Table 3.1. Group of IOD and ENSO using the Niño3 index and DMI	30



전지구 상세기후모델을 이용한 동아시아 여름 몬순에 미치는
IOD와 ENSO 영향에 관한 연구

김 인 원

부경대학교 대학원 환경대기과학과

요 약

이미 예전부터 열대기후와 동아시아 여름 몬순의 경년 변동간의 관계에 대한 다양한 연구가 활발히 진행되어 왔으며, 그 중 태평양을 끼고 있는 동아시아 지역의 여름 몬순의 경년변동과 ENSO (El Niño and Southern Oscillation) 현상과의 관계에 대해 주로 집중되어 왔다. 하지만 최근 거리상으로 동북아시아와 6,000 km 이상 떨어져 있는 인도양의 중요성이 대두됨에 따라 인도양 해수면 온도의 이상 현상인 IOD (Indian Ocean Dipole)와 동아시아 몬순과의 원격 상관에 관한 연구도 눈여겨보고 있다. 따라서 본 연구는 전지구 상세기후 모델을 통해 IOD와 ENSO 현상이 동아시아 여름 몬순 변동성에 미치는 영향에 대해 알아보하고자 30년간 현재기후모의 결과를 이용하여 전지구 상세기후모델이 제안하는 동아시아 몬순에 대한 IOD와 ENSO의 관계를 설명하고자 한다. 또한 추가로 현재기후 분석을 바탕으로 하여, 동아시아 여름 몬순에 작용하는 해수면온도의 역할을 직접적으로 알아보하고자 IOD, ENSO와 관련된 해수면온도 편차를 강제력으로 주어 8개의 민감도 실험을 수행하였다.

먼저 30년 동안의 현재기후 모의분석 결과를 통해 겨울철 IOD지수와 ENSO지수는 한국 지역의 여름철 강수와 양의 상관관계를 보이며, 일본 지역의 여름철 강수와 음의 상관관계가 나타났다. 눈 분석을 통해 IOD는 ENSO현상보다 우리나라와 일본 북쪽 지역의 겨울철 눈 두께간의 높은 상관성을 확인하였으며, 겨울철 눈 두께의 영향이 지속되어 봄철 눈 두께와 일본의 여름철 강수와 양의 상관관계를 가진다. 따라서 모델은 가을에 발달하는 IOD는 겨울부터 봄철까지 한국과 일본 북부지역의 강한 눈을 유발시킴에 따라 이 지역의 여름동안 강한 북풍이 나타나며, 이로 인해 일본지역에 수증기 공급을 방해하여 IOD의 영향이 일본 북부 지역의 몬순활동에 전달하는 역할로 작용할 수 있다고 제안한다.

또한 IOD와 ENSO의 해수면온도 변화 강제력에 따른 민감도 실험 결과로부터 IOD는 동

아시아 지역의 여름몬순 강수와 음의 상관관계를 가지며, IOD는 ENSO현상보다 겨울 및 봄철의 한국과 일본 지역의 눈 두께와 강한 상관관계를 확인할 수 있었다. 이러한 한국과 일본 북부 지역의 눈은 북풍과 함께 한국과 일본 지역으로 건조한 공기의 이동을 유발하며, 적도칭단류를 약화시켜 태평양으로부터의 수증기 공급 방해를 가져온다. 따라서 이러한 대기 순환의 특징은 한국과 일본 지역의 강수 활동 약화시킬 수 있다.



1. Introduction

East Asian summer monsoon (EASM) is a main component of the Asian summer monsoon system and subtropical monsoon including China, Korea and Japan (20°N-45°N, 100°E-140°E). The East Asian summer monsoon plays crucial role on the weather and climate over the regional as well as on a global scale that is quite a complicated system (Xu and Wu 1999). Several studies have also explored that EASM is associated with interannual variability to changes in the Eurasia or Tibetan Plateau snow cover and the Pacific and Indian Ocean Sea Surface Temperature (SST).

Especially in this study we deal with delayed impact of the Pacific and Indian Ocean SST on East Asian summer monsoon. Many studies have cited the El Niño Southern Oscillation (ENSO) phenomenon as the primary factor for the delayed impact on East Asian summer monsoon. Summer rainfall over East Asia region is greatly influenced by the western North Pacific subtropical high (WNPSH) and the intensity of the anomalous WNPSH is a key factor in the EASM variation (Lee et al. 2005). The anomalous Philippine Sea anticyclone conveys impacts of El Niño to East Asian climate during the mature and decay of an El Niño (Wang et al. 2001). However, recent studies have examined influence of the Indian Ocean Dipole (IOD) on EASM. IOD is a coupled ocean-atmosphere phenomenon in the Indian Ocean. It is normally characterized by anomalous cooling of SST in the south eastern equatorial Indian Ocean and anomalous warming of SST in the

western equatorial Indian Ocean. (Saji et al., 1999; Webster et al., 1999; Behera et al., 1999). The different phases of the dipole that different phases of the IOD mode change the intensity of the South Asian High and the western North Pacific subtropical high in summer (Li and Mu 2001). IOD generates a Rossby wave train that causes an extremely hot and dry summer in eastern Asian countries (Guan et al. 2003). SST in the tropical Indian Ocean plays an important role in prolonging the IOD impact on the atmospheric circulation over South and East Asia (Yuan et al. 2008a).

In a follow-up study, Kripalani et al. 2010 is found that positive dipole during autumn could suppress the following summer monsoon activity over East Asia three seasons later in particular over the Korea-Japan sector. Additionally they emphasize that IOD has a stronger relationship with the subsequent summer monsoon precipitation distribution over East-Asia western-North Pacific region than the ENSO phenomenon. However, in previous study, it is difficult to explain the detailed precipitation information due to the limit of data about coarse resolution. Moreover some studies pointed out the increase of the horizontal resolution is crucial for realistic climate simulating using the AGCM. (Deque and Piedelievre, 1995; Stendel and Rockner, 1998; Stratton, 1999).

In this study, we re-examine the relationship of IOD and ENSO on EASM using the global high resolution model GME. First, we have analyzed the present climate simulation and performed sensitivity experiment induced by variation of SST associated IOD and ENSO.

2. Present-day Climate simulation Analysis

2.1 Model description

The higher horizontal resolution has been chosen in order to represent more realistically climate simulation that is supposed to play a crucial role. In this study we have used the GME atmospheric general circulation model (AGCM) (Majewski et al, 2002) with 40 km/40 layers to investigate the relationship of Indian Ocean Dipole (IOD) and El Niño/Southern Oscillation (ENSO) on East Asia Summer Monsoon.

GME is based on an almost uniform icosahedral-hexagonal grid. GME grid point approach also avoids the large amount of global communication required by spectral transform techniques as well as the large number of arithmetic operations normally associated with Legendre transforms at high spatial resolution. A major advantage of the icosahedral-hexagonal grid is the avoidance of the so-called pole problem that exists in conventional latitude-longitude grids. The singularities at the poles lead to a variety of numerical difficulties including a severe limitation on the time step size unless special measures are undertaken. These difficulties simply vanish for grids not having such singularities. To generate the grid, a regular icosahedron is constructed inside the sphere such that 2 of its 12 vertices coincide with the North and South Poles. Five of the other 10 vertices are

spaced at equal longitudinal intervals of $72^\circ (=360^\circ/5)$ along a latitude circle at 26.565°N , the other 5 along a latitude circle at 26.565°S . Connecting nearest neighbors among these 12 points with great circle arcs divides the spherical surface into 20 equal spherical triangles (Fig. 2.1). Beginning from this grid of icosahedral triangles, a new finer grid of triangles is generated by connecting midpoints of the spherical triangle sides by an additional set of great circle arcs (Fig. 2.1b). This process may be repeated until a grid of the desired resolution is obtained (Fig. 2.1c and 2.1d). This construction procedure yields a grid consisting of $10n_i^2+2$ grid points (nodes) and $20n_i^2$ elementary spherical triangles, where n_i is the number of equal intervals into which each side of the original icosahedral triangles is divided. Each of these $10n_i^2+2$ grid points i is surrounded by 6 nearest neighbors except for the original 12 icosahedral vertices, which are surrounded by only 5. We therefore refer to these 12 special points as pentagonal points. If we place all variables at the vertices of the triangles (Arakawa A grid), the dual mesh consists exclusively of hexagons except for the 12 pentagons at the pentagonal points.

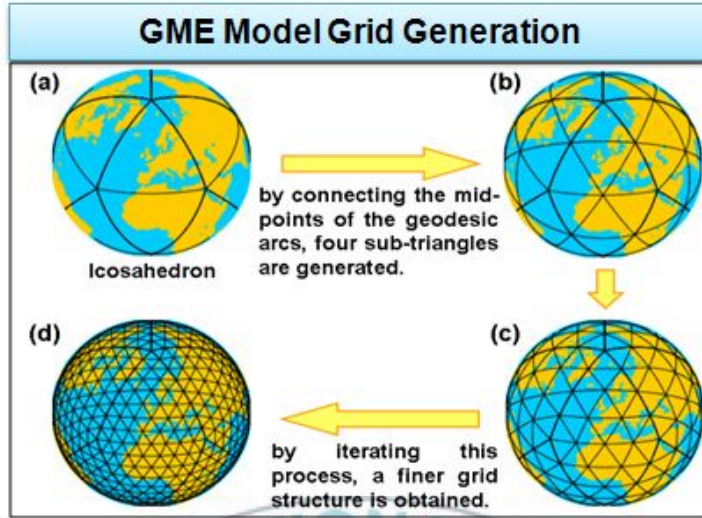


Fig. 2.1 Grid generation by successively halving the triangle edges to form new triangles. Parameter n_i is the number of intervals on major triangle edge.



In the vertical direction, finite differences are applied in a hybrid (sigma pressure) coordinate system to all prognostic variables. The prognostic equations for horizontal velocities, temperature, and surface pressure are solved using a semi-implicit Eulerian approach and for two moisture fields using a semi-Lagrangian scheme to ensure monotonicity and positivity. Prognostic variables are ps , u , v , T , qv , qc , qi , O_3 . Geodesic Model GME generally employs the same methods and procedures as applied in NWP(Numerical Weather Prediction) grid schemes.

Different physical parameterization methods used in GME are summarized in Table 2.1.

Radiation and clouds	Ritter and Geleyn (1992)
Grid-scale precipitation	Doms and Schattler (2003)
Convection	Tiedtke (1989)
Turbulent fluxes in the ABl and the free atmosphere	Muller (1981), based on Louis (1979) Mellor and Yamada (1974)
Soil Model	Heise and Schorodin(2002)
SSo scheme	Lott and Miller (1997)

Table 4.1 Summary of physical parameterization methods in GME

2.2 Data and methodology

The primary datasets used in this study include present-day climate simulation data using the Global model GME. They provide 3 hourly information of 0.4° (longitude and latitude) resolution, covering the time period from 1979 to 2008. Daily climatological AMIP II Sea Surface Temperature and Sea Ice observations have been used for the lower boundary.

To classified the IOD and ENSO, we calculated the seasonal standardized DMI (Dipole Mode Index) and Niño3 index from 1979 to 2008. A year is counted as being a IOD year if the seasonal time series exceeds ± 0.5 for two or more consecutive months between and including June and December. El Niño (La Niña) year is counted if the seasonal time series is larger (smaller) than $+0.5$ (-0.5) for two or more consecutive months between and including June and February of the following year. With these criterion, the years 1982, 1991, 1994, 1997, 2002, 2006, 2007 are identified as positive IOD. In a similar way, the years 1980, 1981, 1984, 1989, 1990, 1992, 1993, 1996, 1998, 2001, 2005 are identified as negative events. The years of positive dipole events associated with El Niño are 1982, 1991, 1997 and the years of positive dipole events associated with La Niña are 1981, 1984, 1992, 1996, 1998. The year of El Niño without IOD events are 1987, 2002 and La Niña without IOD events are 1988, 1999 (Fig. 2.2). In addition some positive IOD events occur during the same year as El Niño, and the same can be said about negative IOD events and La Niña.

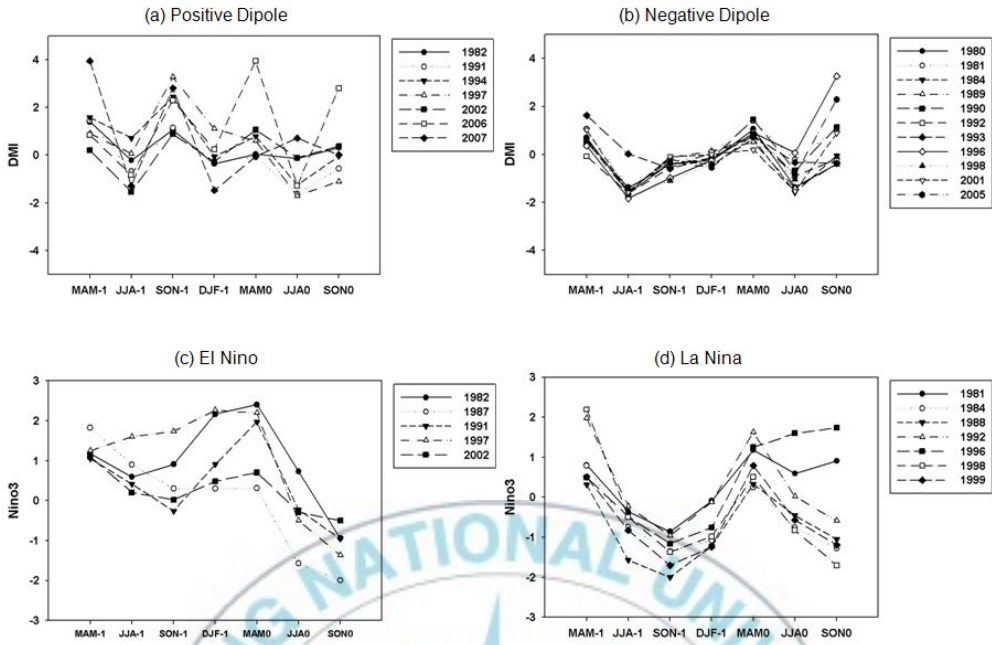


Fig. 5.2 Classification of years when positive or negative IOD and El Niño or La Niña occurred

2.3 Rainfall variability over East Asia

To ascertain EASM inter-annual variability depending on IOD, we analyze accumulated precipitation distribution over East Asia region using the result of model simulation for 30 years period. To get a broader perspective on the surrounding region, differences over the East Asia domain lying between $15^{\circ}\text{N} - 40^{\circ}\text{N}$ and $110^{\circ}\text{E} - 145^{\circ}\text{E}$ are determined. In the discussions to follow, the suffix -1 , 0 and $+1$ with the seasons indicate the seasons for the preceding, concurrent and the following year, respectively, associated with the dipole events.

The composite precipitation differences between positive and negative dipole events for the summer of the concurrent year (JJA0) and for the summer during the following year (JJA+1) are shown in Fig. 2.3. These composites also include ENSO-related years. Fig. 2.4. is same as Fig. 2.3. but for the differences between El Niño and La Niña events. These composites also include IOD-related years. Fig. 2.3. reveals that the positive precipitation anomalies prevail over East Asia domain during JJA0.

However, there is indication of negative precipitation anomalies over Japan and positive anomalies over Korea region during the following summer (JJA+1). Stronger positive precipitation anomalies prevail over East Asia domain during JJA+1 than during JJA0 (Fig. 2.3). Although region of Korea and Japan is adjacent, the phases of anomaly show opposite during JJA+1 (Fig. 2.4). Thus, in this study we especially focus on Korea and Japan area over the East Asia.

Precipitation difference Positive dipole minus Negative dipole

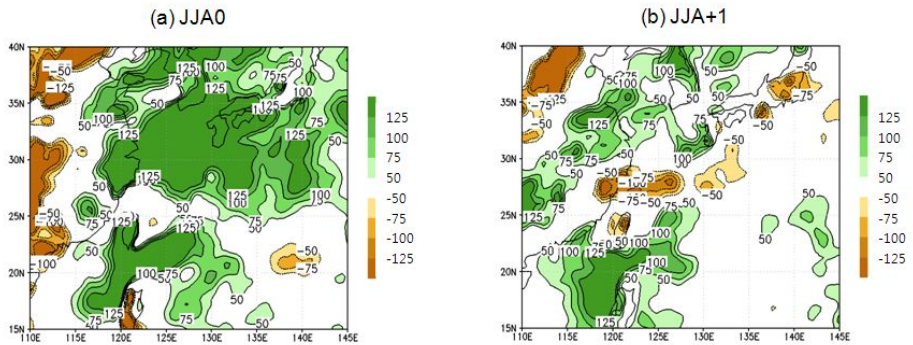


Fig. 2.3 Composite accumulated precipitation anomalies in millimeters for the positive minus negative dipole events; (a) the concurrent year summer (b) following year summer

Precipitation difference El Nino minus La Nina

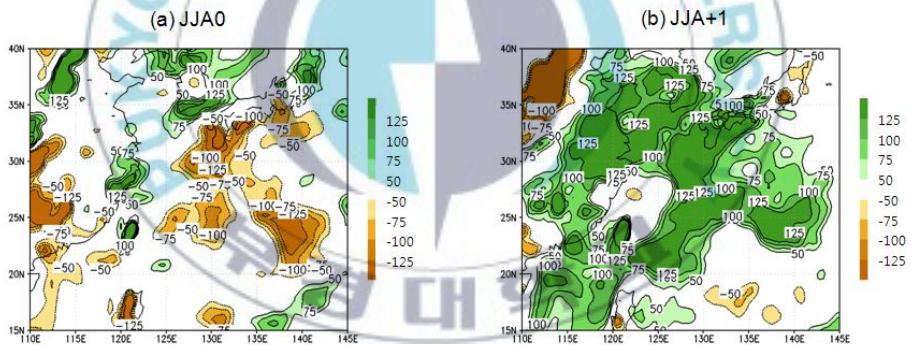


Fig. 2.4 Same as Fig. 2.3. but for the El Niño minus La Niña events; (a) the concurrent year summer (b) following year summer

To ascertain whether the coherent negative precipitation anomalies prevailing over the Japan and positive anomalies over Korea can be related with the IODM and/or ENSO phenomenon, a time series of area-mean summer (JJA+1) precipitation over the sector occupied by intense negative precipitation anomalies over the area A (36°N-40°N, 126°E-129°E) and positive precipitation anomalies over the area B (32°N-38°N, 135°E-144°E) is prepared. Lead/lag CCs are computed between this precipitation time series and indices of the IODM and ENSO phenomena. Since IOD and ENSO sometimes co-occur, we have used a partial correlation analysis to extract a sole influence of IOD and ENSO on East Asian summer monsoon.

The partial correlation measures the degree of association between two random variables, with the effect of a set of controlling random variables removed. Partial correlation coefficient is calculated by Equation (1).

$$PCC_s = r_{XY \cdot Z} = \frac{r_{XY} - r_{XZ}r_{YZ}}{\sqrt{1 - r_{XZ}^2} \sqrt{1 - r_{YZ}^2}} \quad (1)$$

r_{XZ} : *X versus Z correlation*

r_{YZ} : *Y versus Z correlation*

r_{XZ} : *Z versus X correlation*

The partial correlation coefficient between the precipitation with the IODM removing ENSO effect and the precipitation with the ENSO mode removing IODM effect is also computed. For a sample of this size the significant CC is ~ 0.3 at 90% confidence level.

The upper panel of Fig. 2.5 reveals positive relationship of IOD index with subsequent summer monsoon rainfall over Korea. Furthermore, the relation of autumn IOD index with subsequent summer monsoon rainfall over Korea is still similar after the ENSO effect is eliminated. But, this area is not relationship with ENSO.

On the other hand, the lower panel of Fig. 2.5 shows significant negative relationship of ENSO index during SON and IOD index during DJF over Japan. (significant CC at 90% confidence level is ~ 0.3 for a sample of the size) This analysis shows that the IOD might have a stronger relationship with the subsequent summer monsoon precipitation distribution over EAWNP(East Asia-West Pacific) region than the ENSO phenomenon.

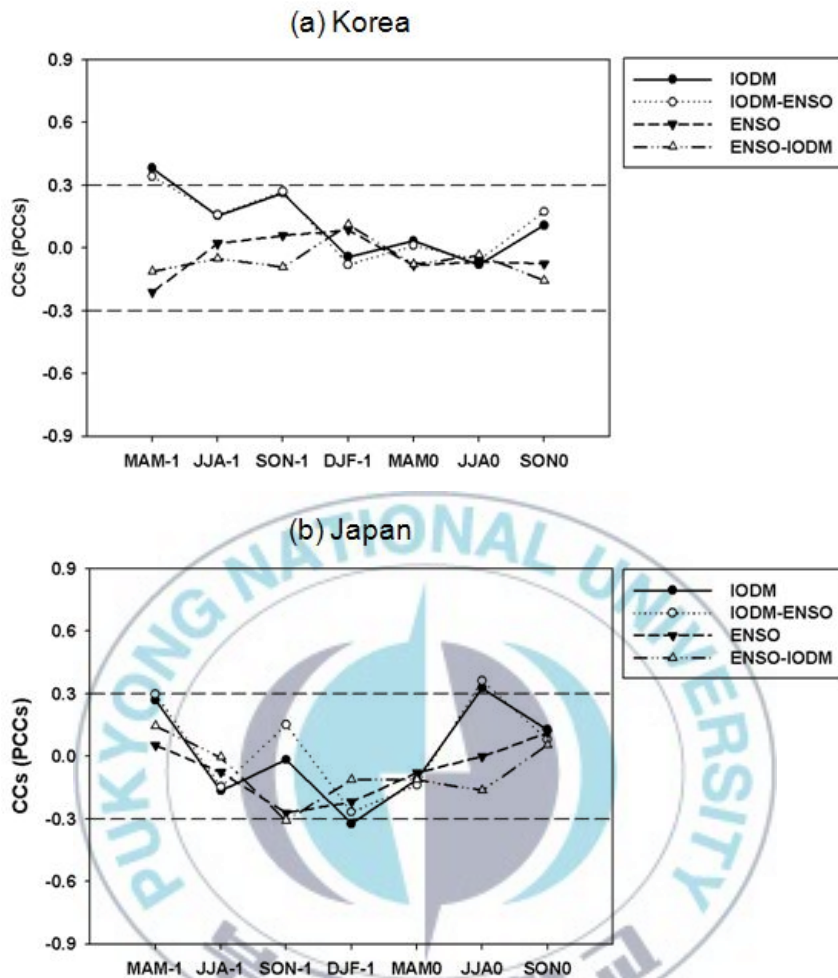


Fig. 2.8 Correlation coefficients between the seasonal IODM and ENSO indices with area-mean summer precipitation; (a) Korea (b) Japan IODM-ENSO (ENSO-IODM) illustrates the partial correlation coefficient with IODM (ENSO) after removing the effect of ENSO (IODM). The seasons on the left (light) of JJA0 indicate indices leading (lagging) summer monsoon precipitation.

2.4 Relationship of IOD and ENSO upon snow depth

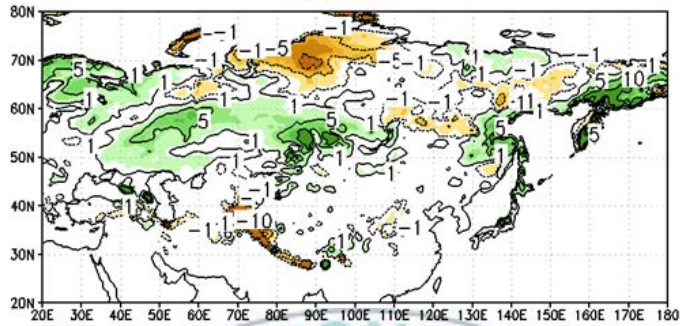
Atmospheric circulation associated with IOD and ENSO does not have such a long memory. However, according to Corti et al. 2000, the large scale long-lasting anomalous circulation system may determine both winter and early spring snow depth anomalies over Eurasia, due to persistence. Kripalani et al. 2005 suggest that delayed influence of positive IOD could be carried by the Eurasian snow via the northern hemisphere mid-latitudes.

Based on the discussion of the above-cited studies, we speculate relationship between snow depth and IOD to explain the delayed impact of IOD and ENSO. The composite snow depth differences between these two sets of extreme dipole events for the following winter and spring have been determined (Fig. 2.6). Positive snow depth anomalies indicating heavy snow have been noted in the north of Korea over the region $50^{\circ}\text{N} - 60^{\circ}\text{N}$, $130^{\circ}\text{E} - 140^{\circ}\text{E}$ and western Eurasia over the region $50^{\circ}\text{N} - 60^{\circ}\text{N}$, $40^{\circ}\text{E} - 100^{\circ}\text{E}$ during the winter and spring season.

Thus this analysis suggests that IOD may be associated with the winter and spring snow distribution over the north Korea and western Eurasia region. In particular, the positive phase of the dipole during summer/autumn may favour heavy snow during the following winter/spring over north of the Korea and western Eurasia.

Composite snow depth difference
for the positive minus negative dipole events

(a) DJF0



(b) MAM+1

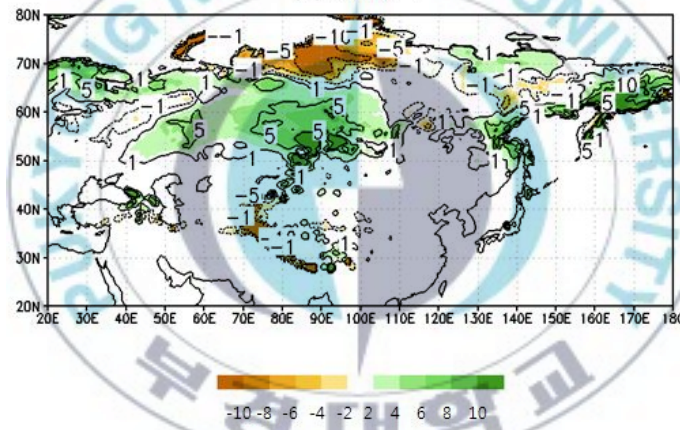


Fig. 2.9 Composite snow depth anomalies in centimeters for the positive minus negative dipole events; (a) DJF0, (b) MAM+1

Again the above composites also contain ENSO-related years. Hence to further ascertain the possible role of the dipole mode on the snow distribution over Korea and western Eurasia region area - mean time series of snow depth during winter (DJF) and spring (MAM) are prepared. (Fig. 2.7 central panel). Again lead/lag CCs are computed between the snow depth time series and indices of the IODM and ENSO phenomena as shown in Fig. 2.7.

To assess the role of the ENSO phenomena in these relations, partial CCs of IODM index with snow depth are determined, after the variance associated with ENSO phenomenon is removed. In DJF, snow depth over area C ($50^{\circ}\text{N} - 60^{\circ}\text{N}$, $40^{\circ}\text{E} - 100^{\circ}\text{E}$) has larger positive relationship with ENSO than IOD (Fig. 2.7b), negative relationship with IOD and ENSO.

On the other hand, snow depth over area D ($50^{\circ}\text{N} - 60^{\circ}\text{N}$, $130^{\circ}\text{E} - 140^{\circ}\text{E}$) during both DJF0 and MAM+1 is significant positive relationship with IOD and ENSO (significant CC at 90% confidence level is ~ 0.3 for a sample of the size). Also CCs of snow depth with IOD is larger than ENSO. Thus, the composite and correlation analyses suggests that the autumn IOD has a stronger relationship with the subsequent winter and spring snow distribution over area D than ENSO phenomenon.

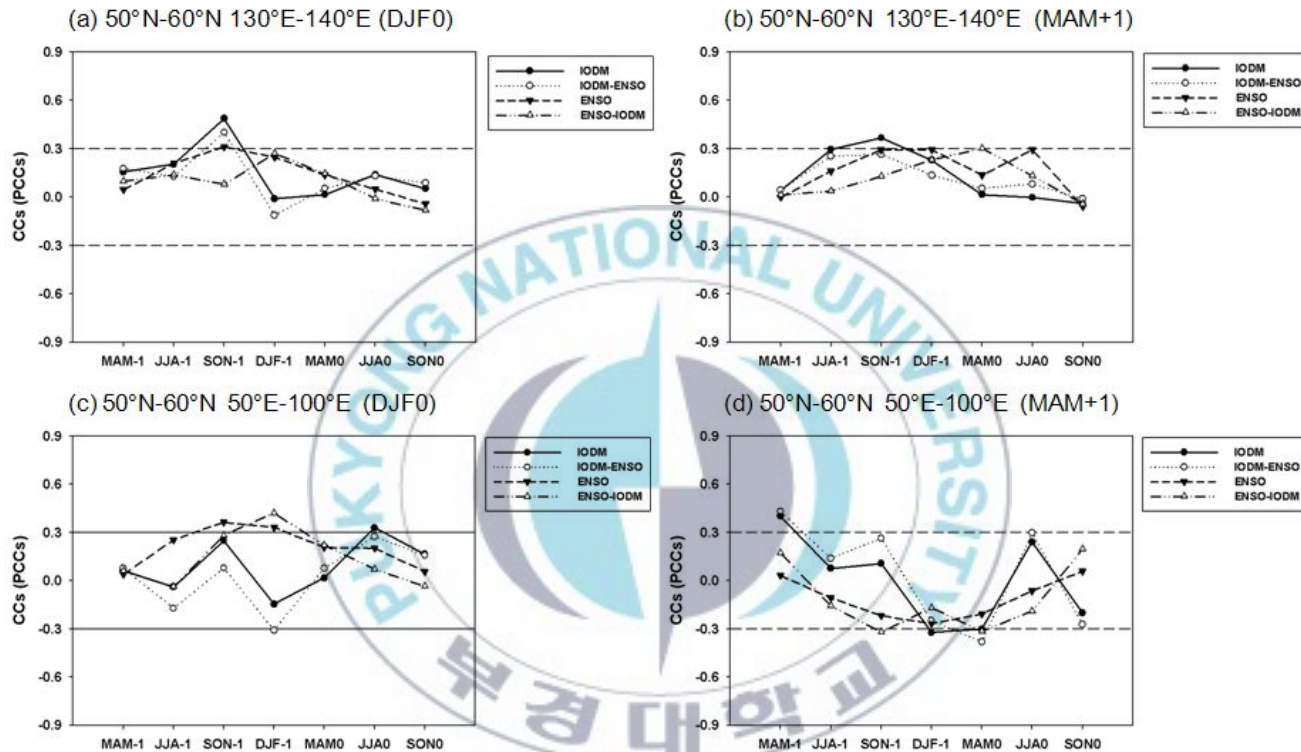


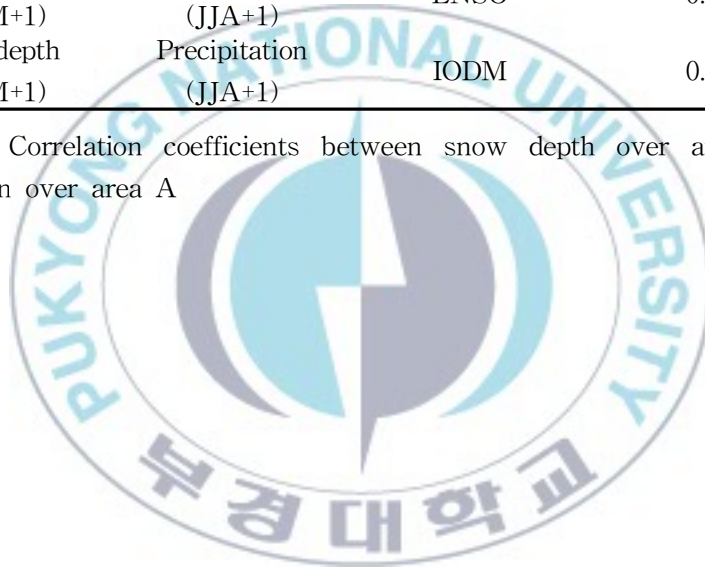
Fig. 2.10 Area-mean winter and spring snow depth; (a) over 50°N-60°N, 130°E-140°E region during the DJF0 , (b) over 50°N-60°N, 130°E-140°E region during the MAM+1, (c) over 50°N-60°N, 40°E-100° E region during the DJF0, (d) over 50°N-60°N, 50°E-100°E region during the MAM+1

2.5 Relationship between snow depth and rainfall

Recently Wu and Kirtman (2007) examined the relationship between winter and spring Eurasian snow with subsequent spring and summer precipitation over East Asia. They suggested that snow and monsoon variability could both be induced by ENSO forcing and the snow - monsoon relationship could be a product of ENSO. They also suggested that snow effects could also be independent of ENSO. To examine this issue, the spring area - mean snow depth over the central Asia and north of Korea and Japan is correlated with area - mean summer precipitation over East asia. Table 2.2, Table 2.3 shows that summer rainfall over both Korea and Japan has no relationship with snow depth over area C during the winter and spring. Table 2.4 also shows that there is no relationship between snow depth over area D summer rainfall over Korea region. But summer rainfall over Japan is significant negative relationship with snow depth over area D in MAM+1. The correlation coefficient between the spring snow and summer precipitation is -0.309 . Once the IOD effect (or ENSO effect) is removed, the partial correlation coefficient is still similar.; significant at 90% confidence level.

Variable1	Variable2	Control variable	CCs (or PCCs)
Snow depth (DJF0)	Snow depth (MAM+1)	-	-0.034
Snow depth (DJF0)	Precipitation (JJA+1)	-	-0.128
Snow depth (DJF0)	Precipitation (JJA+1)	ENSO	-0.061
Snow depth (DJF0)	Precipitation (JJA+1)	IODM	-0.188
Snow depth (MAM+1)	Precipitation (JJA+1)	-	0.234
Snow depth (MAM+1)	Precipitation (JJA+1)	ENSO	0.224
Snow depth (MAM+1)	Precipitation (JJA+1)	IODM	0.212

Table 2.2 Correlation coefficients between snow depth over area C and precipitation over area A



Variable1	Variable2	Control variable	CCs (or PCCs)
Snow depth (DJF0)	Snow depth (MAM+1)	-	-0.034
Snow depth (DJF0)	Precipitation (JJA+1)	-	0.069
Snow depth (DJF0)	Precipitation (JJA+1)	ENSO	0.042
Snow depth (DJF0)	Precipitation (JJA+1)	IODM	0.063
Snow depth (MAM+1)	Precipitation (JJA+1)	-	-0.122
Snow depth (MAM+1)	Precipitation (JJA+1)	ENSO	-0.143
Snow depth (MAM+1)	Precipitation (JJA+1)	IODM	-0.118

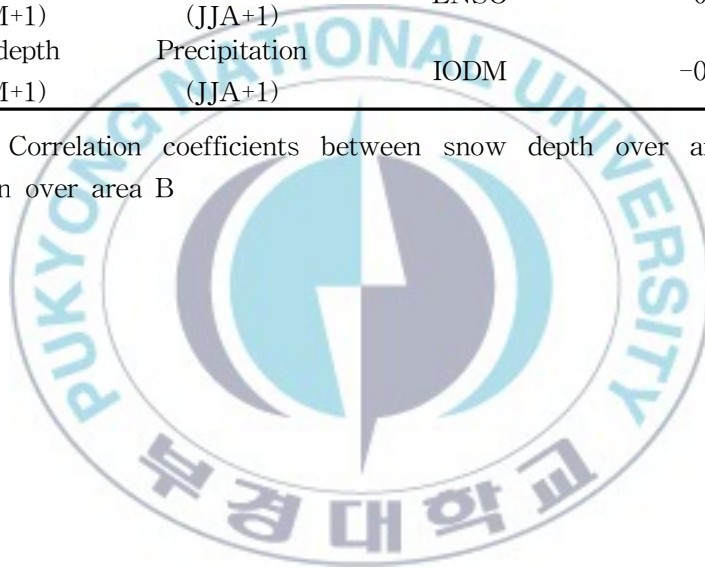
Table 2.3 Correlation coefficients between snow depth over area C and precipitation over area B

Variable1	Variable2	Control variable	CCs (or PCCs)
Snow depth (DJF0)	Snow depth (MAM+1)	-	0.743
Snow depth (DJF0)	Precipitation (JJA+1)	-	0.055
Snow depth (DJF0)	Precipitation (JJA+1)	ENSO	0.035
Snow depth (DJF0)	Precipitation (JJA+1)	IODM	0.054
Snow depth (MAM+1)	Precipitation (JJA+1)	-	0.082
Snow depth (MAM+1)	Precipitation (JJA+1)	ENSO	0.112
Snow depth (MAM+1)	Precipitation (JJA+1)	IODM	0.082

Table 2.4 Correlation coefficients between snow depth over area D and precipitation over area A

Variable1	Variable2	Control variable	CCs (or PCCs)
Snow depth (DJF0)	Snow depth (MAM+1)	-	0.743
Snow depth (DJF0)	Precipitation (JJA+1)	-	-0.107
Snow depth (DJF0)	Precipitation (JJA+1)	ENSO	-0.056
Snow depth (DJF0)	Precipitation (JJA+1)	IODM	-0.117
Snow depth (MAM+1)	Precipitation (JJA+1)	-	-0.309
Snow depth (MAM+1)	Precipitation (JJA+1)	ENSO	-0.300
Snow depth (MAM+1)	Precipitation (JJA+1)	IODM	-0.311

Table 2.5 Correlation coefficients between snow depth over area D and precipitation over area B



2.6 Circulation associated with heavy snow

Recent studies suggest that the large-scale long-lasting anomalous circulation systems and the winter and spring snow depth anomalies over Eurasia are well connected (Ferranti and Molteni, 1999; Kripalani and Kulkarni, 2001; Corti et al., 2000). Snow depth changes are more indicative of changes in the large-scale mid-latitude circulation. This could further affect the land temperature, land-sea temperature contrast and subsequent monsoon strength (Meehl, 1994, 1997). The land-sea temperature contrast plays important role on monsoon. Shukla 1987 hypothesized that an excessive snowfall during the previous winter and spring seasons can delay the build up of the monsoonal temperature gradient because part of the solar energy will be reflected and part will be utilized for melting the snow or for evaporating the soil moisture. A relatively small amount of energy will be left for warming the surface and hence the atmosphere. Snow melting, soil hydrology, change the meridional gradient of the temperature of the land and overlying atmosphere, and in turn affect the development of the following monsoon (Barnett et al. 1989).

In above analysis, the IOD shows significant relationship with snow depth over area D. To examine the circulation patterns associated with the snow depth over the above identified location, composite differences are prepared for heavy minus light snow events. As shown Fig. 2.8 to define the extreme snow events we standardized snow depth from 1979 to 2008 period. After that, we identify heavy (light) snow events

if standardized value exceed +1.0 (-1.0) With this criterion, extreme winter seasons with heavy snow (in the years 1994, 1996, 1997, 2002) and light snow (in the years 1981, 1989, 2005) over area D are identified.

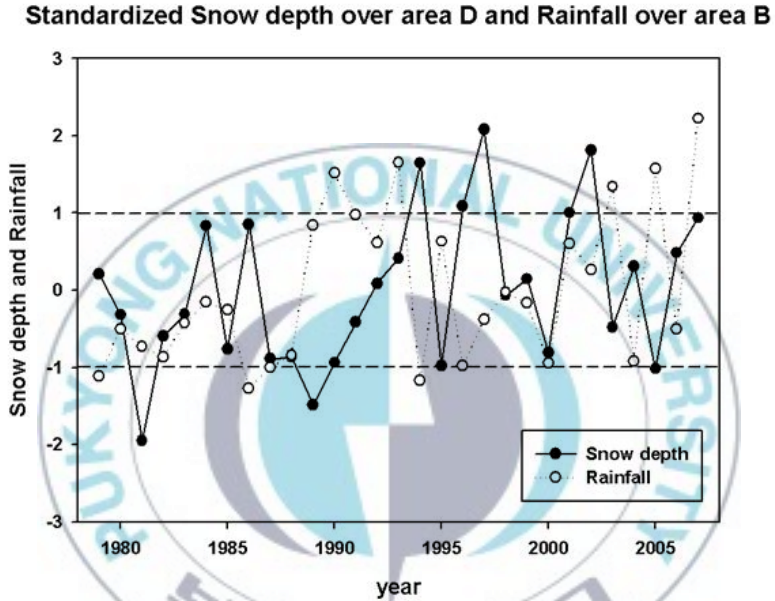
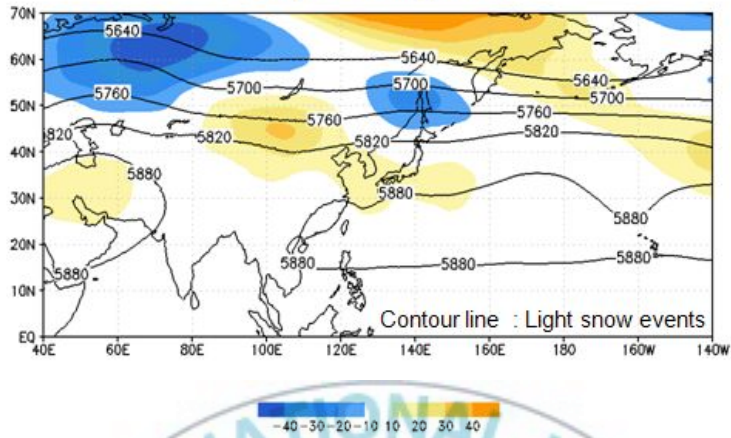


Fig. 2.8 Standardize snow depth over the area D and Rainfall over area B from 1979 to 2008

To examine the circulation patterns associated with the snow depth over the above identified location, composite differences are prepared for heavy minus light snow events. Fig. 2.9 indicate 500 hPa geopotential height differences for the heavy minus light snow events (upper panel) and 850 hPa wind vector differences (lower panel). In case of heavy snow events, 5880 line of geopotential height approach towards Korea region. It means North Pacific Subtropical high is intensified during summer. But there is negative geopotential height differences north of Japan region unlike Korea. Fig. 2.9 (lower panel) reveals that low-level northerly winds over Japan and southerlies over Korea are strong. This northerly winds suppress summer monsoon over Japan since northerly winds over Japan will inhibit the moisture supply towards Japan. On the contrary, southerly winds strengthen the moisture supply towards Korea that intensified summer monsoon rainfall over Korea.

Therefore the circulation anomalies indicate some signals of snow effects. It is interesting to note that the main inferences drawn from Fig. 2.9 are similar to the ones based on the composites of extreme dipole events shown by Kripalani et al 2010. Thus, the similarity of the anomalous mid-latitude circulation patterns associated with the positive dipole mode over the Indian Ocean and heavy snow over area D suggests that they may be inter-linked.

(a) Composite differences of 500hPa Geopotential heights for the extreme snow depth events (JJA+1)
Heavy minus Light snow



(b) Composite differences of 850hPa wind vector (m/s) for the extreme snow depth events (JJA+1)
Heavy minus Light snow

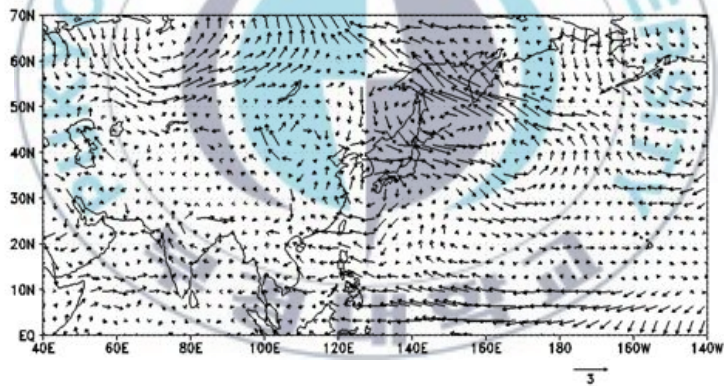


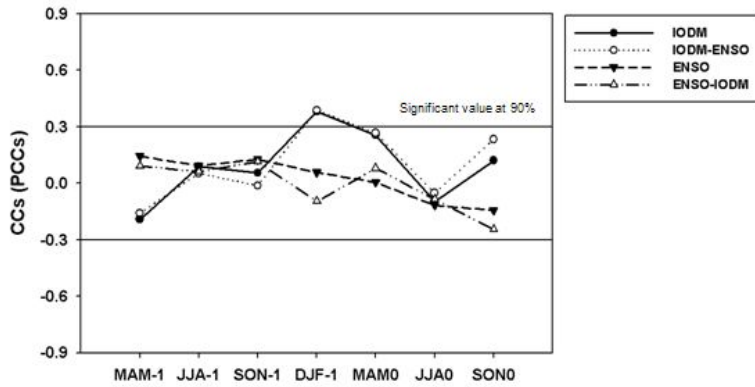
Fig. 2.9 Composite seasonal differences of 500hPa geopotential height in meters for the extreme now depth events (heavy minus light snow over area D)

2.7 Relationship of IOD and ENSO on surface temperature

To ascertain whether the north-south land-sea contrast is an important factor, a time series of area-mean surface temperature anomalies over the East Asia is prepared. As in Fig. 2.5 and Fig. 2.7 correlation and partial correlation analysis of surface temperature over Korea and Japan with the IODM and ENSO indices are presented in Fig. 2.10. shows surface temperature over Korea is stronger positive relationship with IOD in DJF0 than ENSO. Over Japan there is also positive relationship with IOD in DJF0 but, CC_s is smaller than over Korea.

The positive CC_s imply that heavier snow could be associated with higher temperatures over Korea and Japan. It is apparent that heavier snow depth corresponds to lower temperature. Thus the lower temperatures over the north and higher temperatures over the south would increase the meridional temperature gradient resulting in air flow from the northern cooler region to the southern warmer region.

(a) Area A (36°N-40°N 126°E-129°E), JJA+1



(b) Area B (32°N-38°N 135°E-144°E), JJA+1

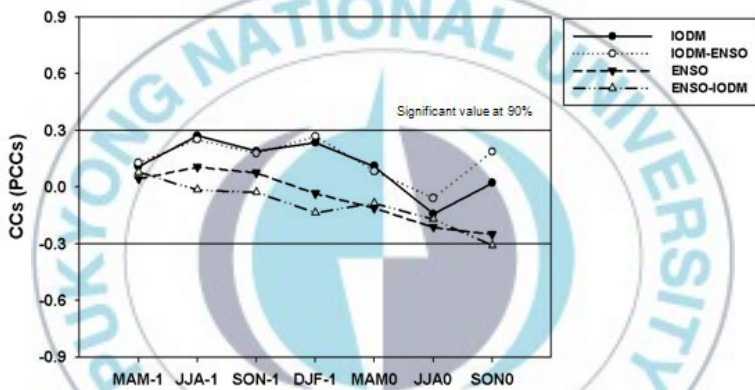


Fig. 2.10 Correlation coefficients between the seasonal IODM and ENSO indices with area-mean summer surface temperature; (a) Korea (b) Japan IODM-ENSO (ENSO-IODM) illustrates the partial correlation coefficient with IODM (ENSO) after removing the effect of ENSO (IODM)

3. Sensitivity experiments

3.1 Experiment design

In this study nine sets of numerical experiments are performed by GME model: the control run with climatological SSTs, and 8 sets of sensitivity experiment with additional forcing from the composite anomalies associated with IOD and ENSO. The nine sets of experiments have been described in Table 3.1. Sensitivity experiments are composed by the runs with SSTs associated with only the positive and only negative phase of the dipole mode (not in concurrence with El Niño/La Niña), runs with SSTs associated with only El Niño or La Niña (not in concurrence with IOD), runs with SSTs associated with positive dipole in concurrence with El Niño, runs with SSTs associated with positive dipole in concurrence with La Niña, runs with SSTs associated with negative dipole in concurrence with El Niño and runs with SSTs associated with negative dipole in concurrence with La Niña.

To identify the sensitivity, we use the observed AMIP II (Atmospheric Model Inter-comparison Project) SST from 1960 to 1999. To determine the SST anomaly patterns associated with the positive and negative phases of the dipole mode, time series of monthly Dipole Mode Index (DMI) and Niño3 has been examined. An index to quantify the IOD has been proposed by Saji et al. (1999). This is the difference in SST anomaly between the western Indian Ocean (50°E–70

°E, 10°S–10°N) and the southeast Indian Ocean (90°E–110°E, 10° S–equator) and is denoted as DMI.

ENSO phenomenon is quantified by the Niño3 Index that is standardized SST anomalies over Niño3 region (5°S–5°N 150°W–90°W). The DMI and Niño3 index calculated from 1960 to 1999 is shown in Fig. 3.2.

	DMI>0.5	-0.5<DMI<0.5	DMI<-0.5
Niño3>0.5	(a) Positive IOD and El Niño	(b) No Dipole and El Niño	(c) Negative IOD and El Niño
-0.5<Niño3<0.5	(d) Positive IOD and Neutral	(e) Climatology	(f) Negative IOD and Neutral
Niño3<-0.5	(g) Positive IOD and La Niña	(h) No Dipole and La Niña	(i) Negative IOD and La Niña

Table 3.1 Group of IOD and ENSO using the Niño3 index and DMI

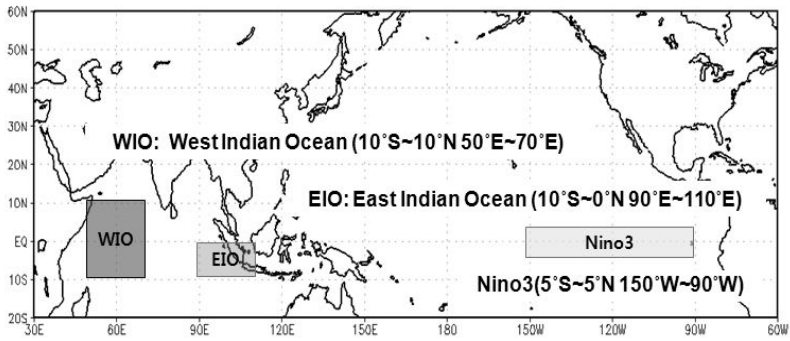


Fig 3.1 Map showing the region of analysis

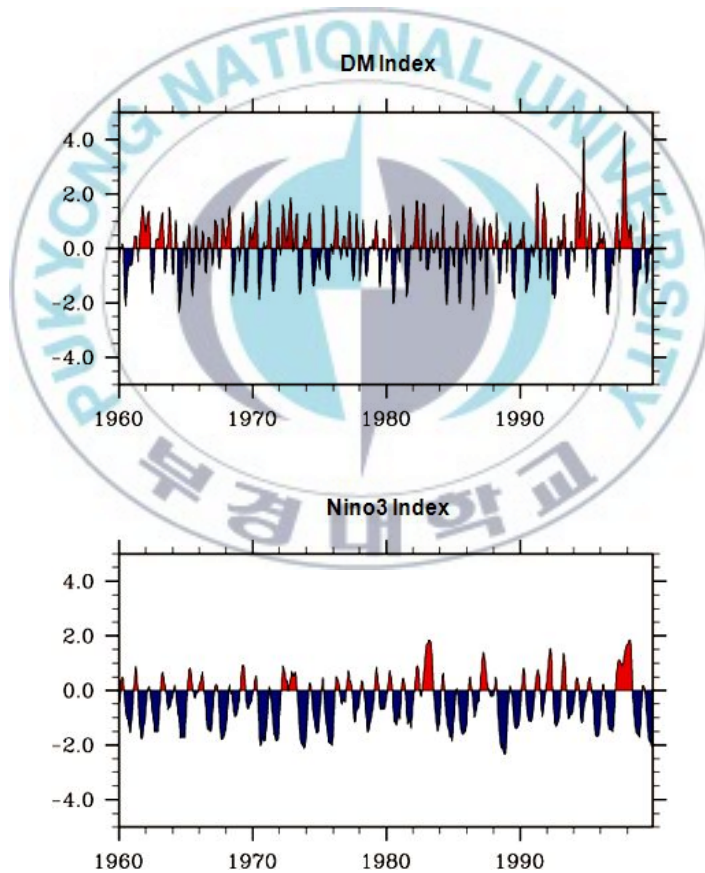


Fig 3.2 IOD Index (upper panel) and Niño3 Index (lower panel) from 1960 to 1999

The SST anomaly pattern (Fig. 3.3 upper panel, left) shows positive anomalies west of 80°E and negative anomalies east of this meridian for the positive phase of the dipole mode in equatorial Indian Ocean. A reverse anomaly pattern is clearly visible for the negative phase of the dipole phenomenon (Fig. 3.3 upper panel, right). (Fig. 3.3 central panel, left) represents El Niño. Significant positive Niño3 SST anomalies are visible in Pacific Ocean. Significant negative Niño3 SST anomalies are visible in Pacific Ocean indicating La Niña (Fig. 3.3 central panel right). These SST patterns (Fig. 3.3 central panel) associated with El Niño and La Niña are independent of IODM. Fig. 3.3 (Lower panel, left) depicts positive IODM event occurring with La Niña. In this case, SST anomaly patterns (Fig. 3.3 lower panel, left) show positive anomalies west of 80°E, negative anomalies east of this meridian and over the entire Pacific Ocean. Similarly a pattern for negative IOD and El Niño has been presented in Fig. 3.3 (Lower panel, right), showing positive SST anomalies east of 90°E, but with some weak negative SST anomalies along 150°E.

SST forcing : 8 Composite SST Anomalies (1960-1999, 40years)

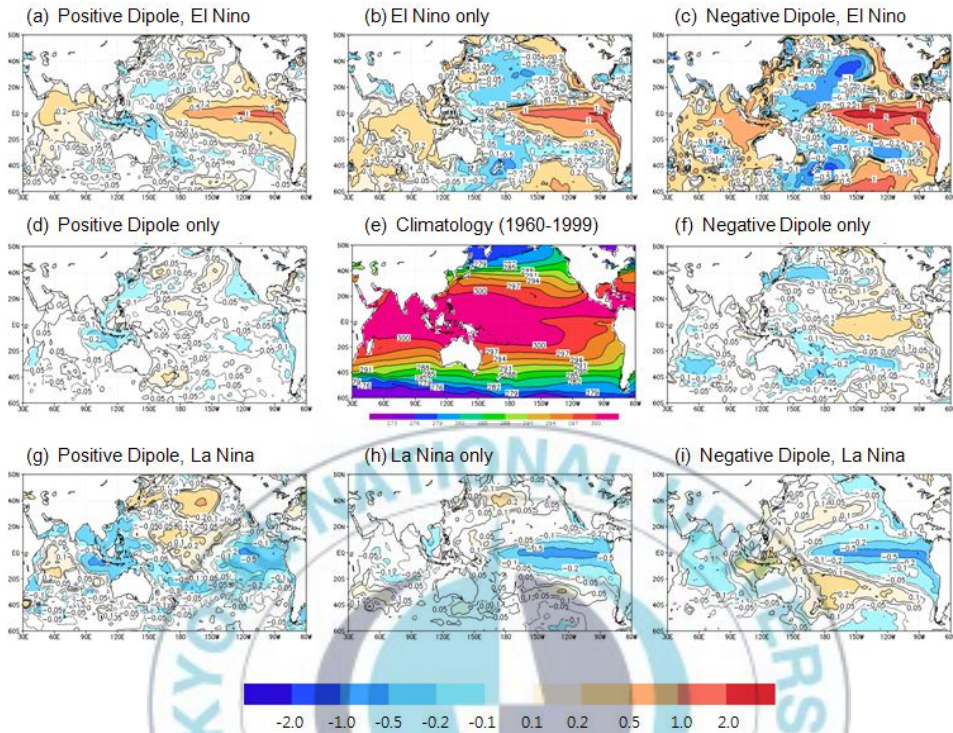


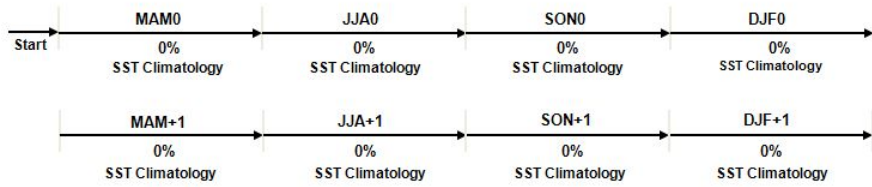
Fig. 3.3. Composite SST anomalies associated with IOD and ENSO; (a) Positive Dipole and El Niño case (b) El Niño only case (c) Negative Dipole and El Niño case (d) Positive Dipole only case (e) Climatology from 1960 to 1999 (f) Negative Dipole only case (g) Positive Dipole and La Niña case (h) La Niña only case (i) Negative Dipole and La Niña case

These SST composites have been super-imposed on the climatological SST patterns for the eight sensitivity experiment. Thus control run is performed with only SST climatology from 1960 to 1999 , and the sensitivity experiments are carried out with additional forcing from the composite anomalies associated with the extreme dipole phases. IOD initiates in summer and peaks in autumn, so the sensitivity experiment was designed in such a way that 50% SST forcing was given in summer, full 100% forcing in autumn, 50% forcing in winter and thereafter experiment continued with climatological SST. (Fig. 3.4.)

Finally we apply to the middle each month, and daily SSTs were obtained by linearly interpolating between these monthly mean values for the boundary condition. After, to reduce the initial transients we conducted procedure of spin-up for one month with initial condition and boundary condition. Model simulation is performed from March for two years.

● SST boundary condition

(a) Control run



(b) 8 cases sensitivity experiment (J.-H. Oh et al. 2005)

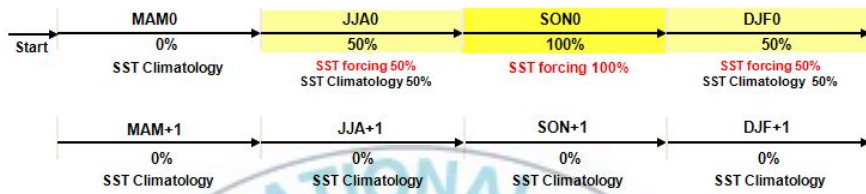


Fig. 3.4 Schematic representation of design of (a) Control run and (b) sensitivity experiments.



3.2 Result of experiments

3.2.1 Rainfall distribution over East Asia

Fig. 3.5 shows rainfall difference in millimeters during the following summer (JJA+1) by present climate simulation (left panel) and sensitivity experiments (right panel). Fig. 3.5a indicates Positive dipole minus Negative IOD phase excluding ENSO and Fig. 3.5b shows El Niño minus La Niña phase excluding IOD. As seen in Fig. 3.5a in case of positive dipole phase present-day climate simulation shows negative anomalies over East Asia and similar with sensitivity experiments.

However the strength of the negative anomalies during sensitivity experiments appear to increase in particular over Korea. As seen in Fig. 3.5b in case of El Niño minus La Niña excluding IOD present-day climate simulation shows positive anomalies over East Asia. But in sensitivity experiments we see the positive and negative anomalies, picture is not clear. Thus with the sensitivity experiments it appear the IOD delayed impact is more than the delayed impact of ENSO.

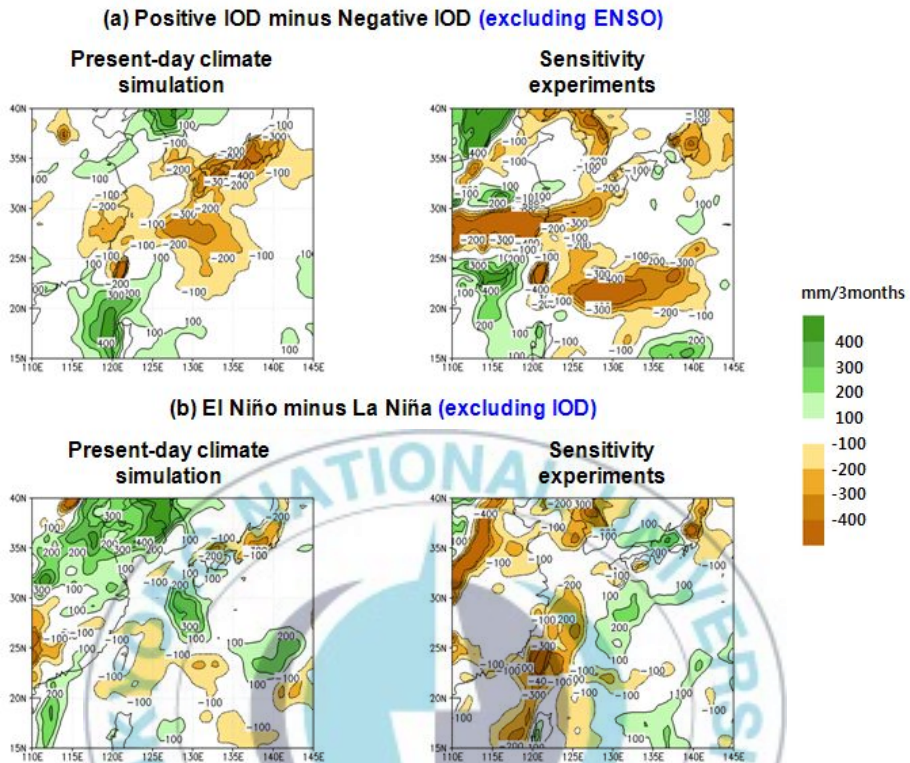


Fig. 3.5 Rainfall difference in millimeters during the following summer (JJA+1) by present climate simulation (left panel) and sensitivity experiments (right panel); (a) Positive dipole minus Negative IOD phase excluding ENSO (b) El Niño minus La Niña phase excluding IOD

3.2.2 Snow depth distribution over East Asia

Fig. 3.6 shows snow depth difference in centimeter during the winter and spring by sensitivity experiments. Upper panel indicates Positive dipole minus Negative IOD phase excluding ENSO and lower panel shows El Niño minus La Niña phase excluding IOD. Comparing upper panel and lower panel we see that more snow is induced over the NH mid-latitudes for the IODM case. If we focus on attention just north of Korea-Japan, we can see positive snow anomalies for the IODM case, but for the ENSO case results are not clear.



Snow depth difference (cm) for the Positive minus Negative dipole events

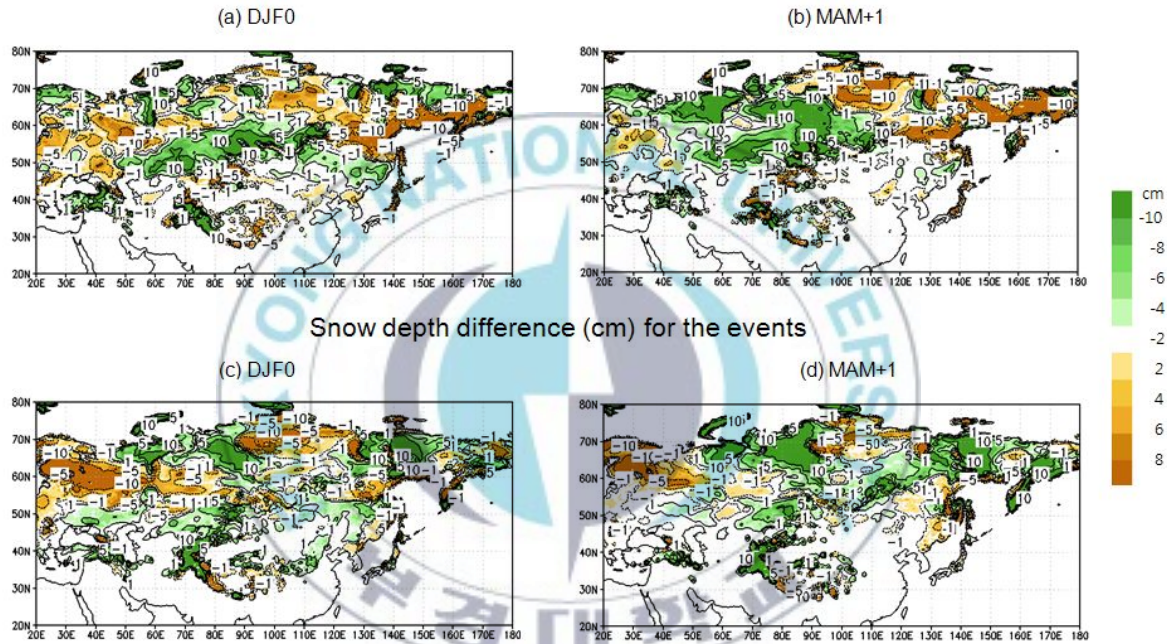


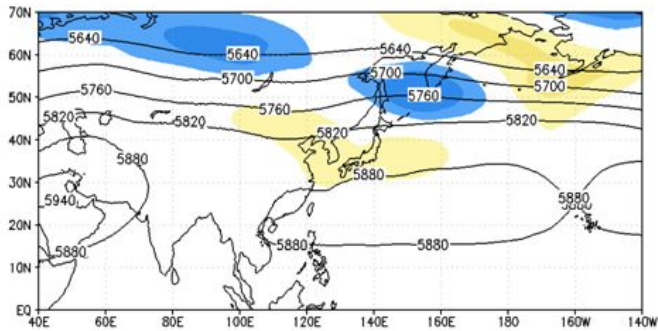
Fig. 3.6 Snow depth difference in centimeter during the winter and spring by sensitivity experiments; Positive dipole minus Negative IOD phase excluding El Niño (upper panel) and El Niño minus La Niña phase excluding IOD (lower panel)

3.2.3 Circulation associated with IOD and ENSO

Fig. 3.7 shows 500 hPa geopotential height difference in meter during the winter and spring by sensitivity experiments. Upper panel indicates Positive dipole minus Negative IOD phase excluding ENSO and lower panel shows El Niño minus La Niña phase excluding IOD. In case of Positive dipole minus Negative IOD there exist positive anomalies over Korea and negative anomalies over north of Japan while in El Niño minus La Niña there are negative anomalies over north of Korea and Japan.

Fig. 3.8 shows 850 hPa Wind vector difference in m/s during the winter and spring by sensitivity experiments. Upper panel indicates Positive dipole minus Negative IOD phase excluding El Niño and lower panel shows El Niño minus La Niña phase excluding IOD. The flow pattern for positive IOD minus negative IOD shows weakening of low level jet which will inhibit transport of moisture from pacific towards Korea and Japan. This may lead to less rainfall. No such feature is clearly seen for the ENSO case.

**(a) Positive IOD minus Negative IOD events
(excluding ENSO)**



**(b) El Niño minus La Niña events
(excluding IOD)**

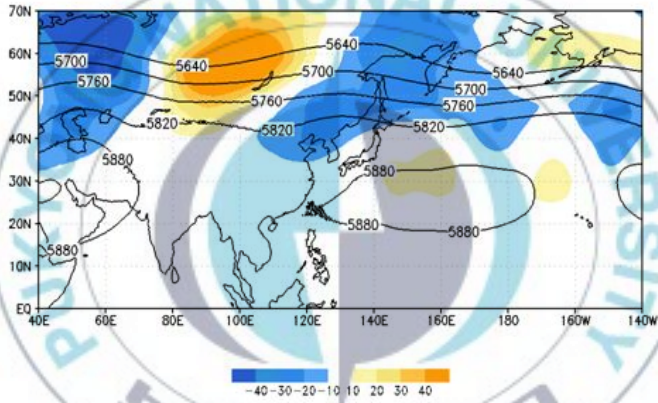
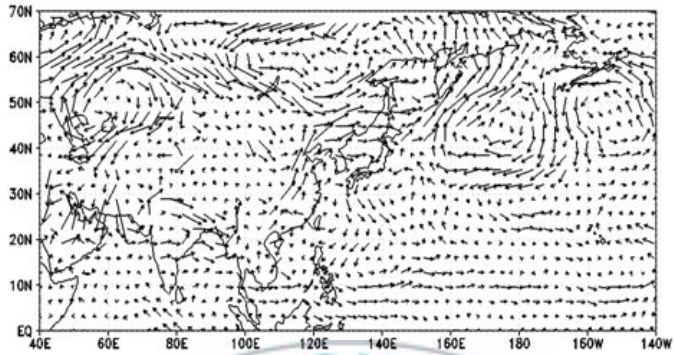


Fig. 3.7 500 hPa geopotential height difference in meter during the Summer by sensitivity experiments; Positive dipole minus Negative IOD phase excluding El Niño (upper panel) and El Niño minus La Niña phase excluding IOD (lower panel)

**(a) Differences of 850 hPa wind vector (m/s)
Positive IOD minus Negative IOD events (JJA+1)**



**(b) Differences of 850 hPa wind vector (m/s)
El Niño minus La Niña events (JJA+1)**

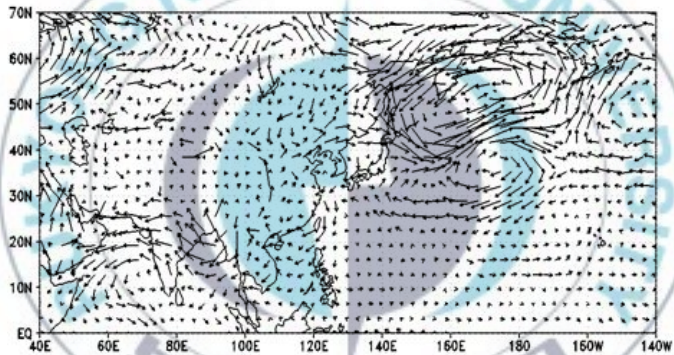


Fig. 3.8 850 hPa Wind vector difference in m/s during the Summer by sensitivity experiments; Positive dipole minus Negative IOD phase excluding El Niño (upper panel) and El Niño minus La Niña phase excluding IOD (lower panel)

4. Summary and Conclusions

In this study, we have re-examined the impact of IOD and ENSO on East Asian summer monsoon, in particular over Korea and Japan. First, we analyze present climate simulation for 1979–2008 to examine relationship IOD and ENSO with EASM through climate model. IOD during the winter shows negative relationship with the following summer monsoon rainfall over Korea and positive relationship over Japan. IOD has a stronger relationship than ENSO with snow depth over the area D during winter. Snow depth over the area D has positive relationship with summer precipitation over Japan. IOD has positive correlation with summer surface temperature over Korea. Model suggests that delayed impact of IOD be carried by the snow distribution over area D. This result in anomalous northerly winds over north Japan during summer, which transports cold and dry air towards Japan. Thus, that leads to suppressed rainfall over Japan.

In addition we carried out sensitivity experiments to verify the impact of SST variability related with IOD and/or ENSO on East Asia summer monsoon. According to sensitivity experiments, IOD has negative relationship with the following summer monsoon rainfall over East Asia in particular Korea–Japan. IOD has a stronger relationship than ENSO with snow depth over the northern hemisphere in particular Korea–Japan during winter and spring. The heavy snow just north of Korea–Japan will induce dry air from north towards Korea–Japan. The weakening of cross-equatorial flow inhibit moisture

supply from the Pacific. All these features could lead to less rainfall activity over Korea-Japan sector.

Consequently high resolution climate model could explain possible mechanism of delayed impact of IOD on East Asian summer monsoon which is suggested by Kripalani et al 2010. But it has limit to verify clearly impact of IOD and ENSO on East Asia summer monsoon only with high resolution climate model. Thus, to improve our understanding of physical mechanism about the result of climate model simulation, various attempt is necessary.



5. References

- 정일웅, 조민수, 임은순, 김정우, 2003: YONU AGCM에서 수평 해상도에 대한 현기후 모사의 민감도. 한국기상학회지, 39(2), 221-237.
- 하경자, 서영경, 서애숙, 정효상, 손병주, 2001: 동아시아 몬순 강수의 경년 변동과 관련된 El Niño와 지표의 상호작용. 한국기상학회지, 37(4), 381-398.
- Ashok, K., Guan, Z., and Yamagata, T., 2001: Impact of the Indian Ocean Dipole on the relationship between the Indian monsoon rainfall and ENSO. *Geophys. Res. Lett.*, 28(23), 4499 - 4502.
- Barnett, T. P., L. Dümenil, U. Schlese, E. Roeckner, M. Latif, 1989: The Effect of Eurasian Snow Cover on Regional and Global Climate Variations. *J. Atmos. Sci.*, 46, 661 - 686.
- Behera SK, Krishnan R, Yamagata T. 1999. Unusual ocean-atmosphere conditions in the tropical Indian Ocean during 1994. *GRL* 26: 3001 - 3004.
- Corti S, Molteni F, Brankovic C (2000) Predictability of snow depth anomalies over Eurasia and associated circulation patterns. *Quart J Roy Meteor Soc* 126: 241 - 262
- Ding, Y., Chan, J. C. L., 2005: The East Asian summer monsoon: an overview. *Meteor. Atmos. Phys.*, 89, 117-142.
- Ding, R., K. J. Ha, Li, J., 2009: Interdecadal shift in the relationship between the East Asian summer monsoon and the tropical Indian Ocean. *Clim. Dyn.*, 34, 1059-1071.
- Déqué, M. and J. P. Piedelievre, 1995: High resolution climate simulation over Europe. *Clim. Dyn.*, 11, 321 - 339.
- Ferranti L, Molteni F (1999) Ensemble simulations of Eurasian snow-depth anomalies and their influence on the summer Asian monsoon. *Quart J Roy Meteor Soc* 125: 2597 - 2610
- Guan Z, Yamagata T. 2003. The unusual summer of 1994 in East Asia: IOD teleconnections. *Geophysical Research Letters* 30.

- Guan, Z., and T. Yamagata, 2003: The unusual summer of 1994 in East Asia: IOD teleconnections. *Geophys. Res. Lett.*, 30, 1544.
- Harou, A. P., Lajoie, R. F., Kniveton, D. R., Frogley, M. R., 2006: The influence of the IODM on precipitation over the Seychelles, *Int. J. Climatol*, 26: 45-54.
- Hong, C.-C., Lu, M.-M., and Kanamitsu, M., 2008: Temporal and spatial characteristics of positive and negative Indian Ocean dipole with and without ENSO. *J. Geophys. Res.*, 113, D08107, doi:10.1029/2007JD009151.
- Iizuka, S., Matsuura, T., and Yamagata, T., 2000: The Indian Ocean SST dipole simulated in a coupled general circulation model. *Geo. Res. Lett.*, 27(20), 3369-3372.
- Kim, B. J., Kripalani, R. H., Oh, J. H., Moon, S. E., 2002: Summer monsoon rainfall over South Korea and associated circulation features. *Theor. Appl. Climatol.*, 72, 65 - 74.
- Kripalani RH, Kulkarni A (2001) Monsoon rainfall variations and teleconnections over South and East Asia. *Int. J. Climatol* 21: 603 - 616
- Kripalani, R. H., Oh, J. H., Kang, J. H., Sabade, S. S., and Kulkarni, A., 2005: Extreme monsoons over East Asia: Possible role of Indian Dipole Mode. *Theor. Appl. Climatol.*, 82, 81-94.
- Kripalani, R. H., J. H. Oh, and H. S. Chaudhari, 2010: Delayed influence of the Indian Ocean Dipole mode on the East Asia - West Pacific monsoon: Possible mechanism, *Int. J. Climatol.*, 30, 197 - 209, doi:10.1002/joc.1890.
- Lee E-J, Jhun J-G, Park C-K (2005) Remote connection of the northeast Asian summer rainfall variation revealed by a newly defined monsoon index. *J Clim* 18:4381 - 4393
- Li, H., A. Dai, T. Zhou, and J. Lu, 2008: Responses of East Asian summer monsoon to historical SST and atmospheric forcing during 1950 - 2000, *Clim. Dyn.*, in press, doi:10.1007/s00382-008-0482-7.
- Li, T., Wang, B., Chang, C.-P, and Zhang, Y., 2003: A Theory for the Indian Ocean Dipole-Zonal Mode. *J. Atmos. Sci.*, 60, 2119 - 2135.
- Li, C.-Y., and Mu, M.-Q., 2001: The influence of the Indian Ocean dipole on

- atmospheric circulation and climate, *Adv. Atmos. Sci.*, 18(5), 831-843.
- Majewski, D., Liermann, D., Prohl, P., Ritter, B., Buchhold, M., Hanisch, T., Paul, G., and Wergen, W., 2002: The operational global icosahedral-hexagonal gridpoint model GME: Description and high-resolution tests. *Mon. Wea. Rev.*, 130, 319-338.
- Merkel, U., and Latif, M., 2002: A high resolution AGCM study of the El Niño impact on the North Atlantic/European sector. *Geophys. Res. Lett.*, 29(9), 1291.
- Saji, N. H., Goswami, B. N., Vinayachandran, P. N., and Yamagata, T., 1999: A dipole mode in the tropical Indian Ocean. *Nature*, 401, 360-363.
- Saji, N. H. and Yamagata, T., 2003: Possible impacts of Indian Ocean Dipole mode events on global climate. *Clim Res*, 25(2), 151-169.
- Stendel, M. and E. Röckner 1998: Impacts of horizontal resolution on simulated climate statistics in ECHAM4. MPI report 253, MPI, Hamburg, Germany.
- Stratton, R.A. 1999a: A high resolution AMIP integration using the Hadley Centre model HadAM2b. *Clim. Dyn.*, 15, 9 - 28.
- Stratton, R.A. 1999b: The impact of increasing resolution on the HadAM3 climate simulation. HCTN 13, Hadley Centre, The Met. Office, Bracknell, UK.
- Taylor, K. E., D. Williamson, and F. Zwiers, 2000: The sea surface temperature and sea-ice concentration boundary conditions of AMIP II simulations. PCMDI Rep. 60, 20 pp.
- Wang, Y., B. Wang, and J. H. Oh, 2001: Impact of the preceding El Niño on the East Asian summer atmosphere circulation. *J. Meteor. Soc. Japan*, 79, 575 - 588.
- Webster PJ, Moore AM, Loschnigg JP, Leben RR. 1999. Coupled ocean-atmosphere dynamics in the Indian Ocean during 1997 - 1998. *Nature* 401: 356 - 360.
- Wu, R. and Wang, B., 2002: A contrast of the East Asian summer monsoon-ENSO relationship between 1962-77 and 1978-93. *J. Climate.*,

15, 3266-3279.

- Wu R, Kirtman BP. 2007. Observed relationship of spring and summer East Asian Rainfall with winter and spring Eurasian snow. *Journal of Climate* 20: 1285 - 1304
- Xu, J., and G. X. Wu, Dynamics of Asian summer monsoon and its maintenance mechanism, *Adv. Atmos. Sci.*, 16, 523-536, 1999
- Yamagata, T., Behera, S. K., Rao, S. A., Guan, Z., Ashok, K., and Saji, N. H., 2002: The Indian Ocean dipole: a Physical Entity, *CLIVAR Exchanges*, 24, 15-18.
- Yang, M., Ding, Y., Li, W., Mao, H., and Huang, C., 2007: The Leading Mode of Indian Ocean SST and Its Impacts on Asian Summer Monsoon.
- Yang, J., Liu, Q., Xie, S.-P., Liu, Z., and Wu, L., 2007: Impact of the Indian Ocean SST basin mode on the Asian summer monsoon. *Geophys. Res. Lett.*, 34.
- Yuan, Y., Yang, H., Zhou, W., Li, C. Y., 2008: Influences of the Indian Ocean dipole on the Asian summer monsoon in the following year. *Int. J. Climatol.*, 28, 1849-1859.
- Yuan, C., Tozuka, T., Miyasaka, T., Yamagata, T., 2009: Respective influences of IOD and ENSO on the Tibetan snow cover in early winter. *Clim. Dyn.*, 33, 509 - 520.